JOURNAL OF SOLID STATE CHEMISTRY **102,** 501–518 (1993)

Crystal Structures of Ca-Free $Pb_2Sr_2RCu_3O_8$ (R = La, Pr, Nd, Eu, Tb, and Dy) Single Crystals

J. S. XUE,* J. E. GREEDAN, AND M. MARIC

Institute for Materials Research, McMaster University, Hamilton, Ontario, Canada L8S 4M1

Received April 29, 1992; accepted July 17, 1992

Structures of $Pb_2Sr_2RCu_3O_8$ have been determined by single crystal X-ray diffraction. A monoclinic symmetry ($C2/m$, $Z = 2$) was found for those crystals with R = Pr, Nd, and Tb, orthorhombic ($Cmmm$, $Z = 2$) for R = La, and tetragonal ($P4/mmm$, $Z = 1$) for R = Eu and Dy. The relationship among different crystal symmetries can be understood in terms of different oxygen orderings in the PbO layers driven by the Pb^{2+} lone pair orientation. There is evidence for $a \sim 9\%$ deficiency in electron density at the R = Eu and Dy sites (and ~4.5% for R = Tb) which has been confirmed by mass spectroscopy as being due to cation vacancies at these sites. Bond valence sum calculations have been performed to evaluate the strains existing in the crystal structures of $Pb_2Sr_2RCu_3O_8$.

I. Introduction

The first compound to have been discovered in the now extensive lead cuprate system of superconducting oxides, $Pb_2Sr_2Y_{1-x}Ca_xCu_3O_{8+\delta}$, or the Pb-2213 phase, continues to be of interest (*1*). Recently, high quality single crystals of the Ca-doped 2213 phase were grown by a PbO/NaCl flux technique (*2*). The best crystals showed $T_c > 80$ K for $x \approx 0.3$ and were of sufficient size and of convenient habit to allow determination of the anisotropy in the basic superconducting parameters such as penetration depth, coherence length, and critical fields using dc-resistivity, magnetization, and optical measurements (*3*). It is generally regarded that the hole-doping mechanism in this system is the substitution of Ca for Y which, for $x = 0.3$ and assuming eight oxygens per formula unit, gives a formal oxidation state of +2.15 for copper, while for Ca-free samples, or the so-called prototype 2213-phase, the oxidation state is of course +2.00. Indeed, Ca-free $Pb_2Sr_2YCu_3O_8$ has been found to be an insulator by several groups (*4–6*). Bulk superconductivity (T_c = 10 to 70 K) in Ca-free 2213 single crystals was first reported by Cava *et al.* (*4*) without further detailed study of the crystal structure and physical properties of these materials. Schneemeyer *et al.* (*7*) substituted various rare-earth elements (R) into the Y-sites and the resultant polycrystalline compounds $Pb_2Sr_2RCu_3O_8$ showed only a small amount of superconductivity (1% or less) ascribed by the authors to variations in the oxygen content or to inhomogeneities. Later, Prasad *et al.* (*8*) reported the existence of superconductivity (T_c = 70 K) in $Pb_2Sr_2RCu_3O_8$ (R = any rare-earth except for La and Ce) powder samples with a low superconducting volume fraction (≤10%). Thus the situation

* Current address: Chemistry Division, Argonne National Lab. 9700 S. Cass Ave. Argonne, IL 60439, USA.

0022-4596/93 $5.00

regarding the Ca-free 2213 phase is presently unclear.

Bulk superconductivity in $Pb_2Sr_2YCu_3O_8$ single crystals was detected in our laboratory a year ago. In order to understand this result, a systematic study of the crystal growth, structural characterization, and physical properties of the $Pb_2Sr_2RCu_3O_8$ (R = La, Ce, Pr, Nd, Sm, Eu, Gd, Tb, Dy, Ho, and Y) single crystal series has been carried out. This series turns out to be an ideal system for studying the relationship between crystal structure and the electronic properties of high-T_c copper oxide superconductors, since these $Pb_2Sr_2RCu_3O_8$ crystals display a systematic trend from insulating to metallic and superconducting character as a function of decreasing rare-earth size. Crystals with R = La, Ce, Pr, and Nd exhibit an insulating behavior with basically no carrier-doping in the CuO_2 planes; R = Sm, Eu, Gd, and Tb are lightly doped; and R = Dy, Ho, and Y are poor metals. The crystals with medium and small rare-earth elements (i.e., R = Eu, Gd, Dy, Ho, and Y) all show a superconducting transition around 70 K with the exception of crystals with R = Tb which are nonsuperconducting due to either a low doping level or to a small portion of the Tb ions present in the +4 oxidation state. Results of dc resistivity and optical reflectivity measurements on these Ca-free $Pb_2Sr_2RCu_3O_8$ single crystals have been reported (*9*). The crystal growth and studies of the relationship between cation vacancies and the electronic properties will be presented in the accompanying paper (*10*). This paper focuses mainly on the crystal structures of $Pb_2Sr_2RCu_3O_8$ which have been determined on samples with R = La, Pr, Nd, Eu, Tb, and Dy by single crystal X-ray diffraction, addresses the question of crystal symmetries, and outlines the evidence for cation vacancies at the rare-earth sites for R = Eu, Tb, and Dy. The inherent strains in the crystal structure have been analyzed in terms of bond valence sum calculations.

II. Experimental

A typical crystal structure determination started with choosing a small, brick-shaped $Pb_2Sr_2RCu_3O_8$ crystal in order to minimize X-ray absorption which is serious for these compounds. The linear absorption coefficient of $Pb_2Sr_2LaCu_3O_8$ is 57.17 mm^{-1} for a silver radiation source with a wavelength of 0.56086 Å. The data sets were collected for $Pb_2Sr_2RCu_3O_8$ (R = La, Pr, Nd, Eu, Tb, and Dy) on a Siemens $P3$ single crystal X-ray diffractometer. The crystal faces were indexed after data collection and the shapes of the crystals were examined under an optical microscope (Olympus BH-2) and recorded by a video camera so that the dimensions of the crystals could be measured on a magnified view from a TV screen giving an accuracy of ± 0.7 μm. A face-indexed numerical absorption correction was then performed. Details of the data collection and crystallographic information for six $Pb_2Sr_2RCu_3O_8$ (R = La, Pr, Nd, Eu, Tb, and Dy) crystals are given in Table I.

1. $Pb_2Sr_2RCu_3O_8$ (R = Pr, Nd, and Tb)

Small monoclinic distortions were detected in several $Pb_2Sr_2RCu_3O_8$ (R = Pr, Nd, and Tb) crystals by the single crystal X-ray diffractometer. In the case of the R = Nd crystal, the monoclinic lattice parameters were refined from 35 centered reflections within the 2θ range from 15° to 40° using an auto-indexing package supplied by Siemens. A data set was collected on a primitive lattice within a hemisphere. Direct methods were applied to locate the metal positions in the unit cell and a full-matrix least-squares refinement was carried out by minimizing $\Sigma w(F_0 - F_c)^2$ using the SHELXTL-PLUS(VMS) package. Out of a total of 2024 independent reflections, 117 were

TABLE I

SUMMARY OF CRYSTALLOGRAPHIC INFORMATION FOR $Pb_2Sr_2RCu_3O_8$ (R = La, Pr, Nd, Eu, Tb, and Dy)

R:	La	Pr	Nd	Eu	Tb	Dy
Dimensions (mm^3)	0.172 × 0.167 × 0.005	0.100 × 0.100 × 0.031	0.131 × 0.122 × 0.100	0.147 × 0.136 × 0.072	0.153 × 0.112 × 0.027	0.124 × 0.117 × 0.069
Diffractometer			Siemens P3			
Radiation			Ag K_α(λ = 0.56086Å)			
Monochromator			Graphite			
Temperature			Ambient			
Absorption correction			Face-indexed numerical			
Scan mode			θ–2θ			
2θ range (°)	3–80	3–80	3–60	3–80	3–70	3–80
Octants	+++	+++−−+	+++−++	+++−−+	++−−++	++−−−+
		−++−−+	−−++−+		−−+−+	
Crystal system	Orthorhombic	Monoclinic		Tetragonal	Monoclinic	Tetragonal
Space group	*Cmmm*(65)	*C*2/*m*(12)		*P*4/*mmm*(123)	*C*2/*m*(12)	*P*4/*mmm*(123)
a (Å)	5.460(1)	5.456(2)	5.443(2)	3.846(2)	5.407(1)	3.833(1)
b (Å)	5.505(1)	5.481(2)	5.468(2)		5.446(1)	
c (Å)	15.876(3)	15.804(5)	15.774(3)	15.786(5)	15.742(2)	15.756(5)
β (°)	90.0	90.18(3)	90.13(2)	90.0	90.41(1)	90.0
Density (g/cm^3)	7.29(Z = 2)	7.37(Z = 2)	7.45(Z = 2)	7.38(Z = 1)	7.58(Z = 2)	7.56(Z = 1)
Formula weight	1047.2	1049.2	1052.5	1045.9	1058.4	1056.2
Max/Min transmission	0.866/0.121	0.382/0.065	0.133/0.037	0.168/0.032	0.411/0.050	0.198/0.065
Extinction (μm)	0.0001(1)	0.0001(1)	0.0001(1)	0.0003	N/A	0.0037
Total reflections	2755	1412	6084	2426	3425	1958
Independent reflections	1412	1195	2024	987	1856	980
R_{int} (%)	1.30	3.03	5.83	3.94	3.49	2.95
Obs. reflections [$I > 3\sigma(I)$]	422	523	1204	465	1143	496
Data/parameters	11.4	10.3	23.2	16.6	21.6	17.7
μ(mm^{-1})	57.170	58.363	59.088	59.936	61.538	61.663
R (%)	5.45	3.80	4.52	4.22	2.83	4.15
R_w (%)	7.89	3.87	5.04	4.77	3.19	5.84
Goodness of fit, S	1.62	1.78	2.02	1.47	1.32	0.79
Max shift/ESD	0.001	0.001	0.001	0.001	0.001	0.001

found which violate the C-centering condition $h + k = 2n$, and 72 of them had an integrated intensity greater than $3\sigma(I)$ suggesting a primitive lattice. The systematic extinctions of $0k0$: $k = 2n + 1$ and $h0l$: $h = 2n + 1$ are consistent with the space group $P2_1/a$ (No. 14). However, the structure refinement performed on this space group was not very successful: the thermal parameters of the oxygens could only be refined isotropically (otherwise, they became nonpositive definite) and the R indices were $R = 7.80\%$ and $R_w = 7.76\%$, respectively. Strong correlations with the correlation coefficients ranging from 0.71 to 0.92 were observed in both the z coordinates and the anisotropic thermal parameters between the oxygens at $(\frac{1}{4}, \frac{1}{4}, z)$ and $(\frac{3}{4}, \frac{3}{4}, z)$ in the CuO layers, implying a higher symmetry space group. Refinement in $C2/m$ (No. 12) was successfully conducting by omitting those weak $h + k = 2n + 1$ reflections which presumably originate from the oxygen ordering in the PbO layers and will be discussed in more detail later in this text. Refinements on $Pb_2Sr_2RCu_3O_8$ with R = Pr and Tb were similar except that an electron density deficiency of ~4.5% was found at the Tb site. The best result was achieved in the case of R = Tb (see Table I for R indices). The unit cell is shown in Fig. 1c.

2. $Pb_2Sr_2LaCu_3O_8$

In contrast, there was no monoclinic distortion observed in the $Pb_2Sr_2LaCu_3O_8$ crystal. The lattice parameters $a = 5.460(1)$ Å, $b = 5.505(1)$ Å, $c = 15.876(3)$ Å, $\alpha = 90.00(1)°$, $\beta = 90.03(1)°$, and $\tau \times 90.02(1)°$ were obtained from a thin plate of $Pb_2Sr_2LaCu_3O_8$ using 38 centered reflections with 2θ ranging from 15° to 30° indicating an orthorhombic cell. A data set was collected from the primitive lattice type within one octant. There were 143 out of a total of 1412 independent reflections violating the C-centering condition, but only 61 of them had an integrated intensity greater than $3\sigma(I)$. The intensities of these reflections are relatively weak [$1 \sim 13\sigma(I)$]. The same crystal was mounted on a precession camera and exposed for 4 days and none of these weak reflections appeared on the film. The space group of $Pman$, which is a nonstandard setting of $Pmna$ (No. 53), was deduced from the systematic absences of $hk0$: $h + k = 2n + 1$ and $h0l$: $h = 2n + 1$. The structure refinement was performed by using the reported atomic coordinates (*11*) as the starting values, except that the position $8i$ (x, y, z) was assigned to the oxygens (O3) in the PbO layers in our refinement instead of to the $4h$ $(0, y, z)$ as in Ref. (*11*). The anisotropic thermal parameters of O3 thus obtained were basically isotropic. However, the refinement result was unsatisfactory since a situation was encountered similar to that in the monoclinic case, i.e., strong correlations and nonpositive definiteness of the thermal parameters of oxygens. Therefore, as in the previous cases, the higher symmetry space group, $Cmmm$ (No. 65), was used. The refinement results (see Tables II and III) resemble those of the monoclinic cases except that the O3 in the PbO layers were split into four closely spaced sites instead of two as in the latter. The occupancies of both the rare-earth and the O3 were refined to full and quarter occupations, respectively, and were subsequently fixed at these values in the final refinement. The unit cell is shown in Fig. 1b.

3. $Pb_2Sr_2RCu_3O_8$ (R = Eu and Dy)

The structure refinements of the $Pb_2Sr_2RCu_3O_8$ (R = Eu and Dy) crystals proceeded somewhat differently from those with R = La, Pr, Nd, and Tb. A primitive, tetragonal cell was found for a $Pb_2Sr_2EuCu_3O_8$ crystal from 25 centered reflections. The attempt to transform the small, primitive cell ($a_p \approx 3.84$ Å) to a conventional cell with $a = \sqrt{2}a_p \approx 5.4$ Å was made by collecting a small data set of 500 reflections with 2θ ranging from 4° to 45° in the one octant.

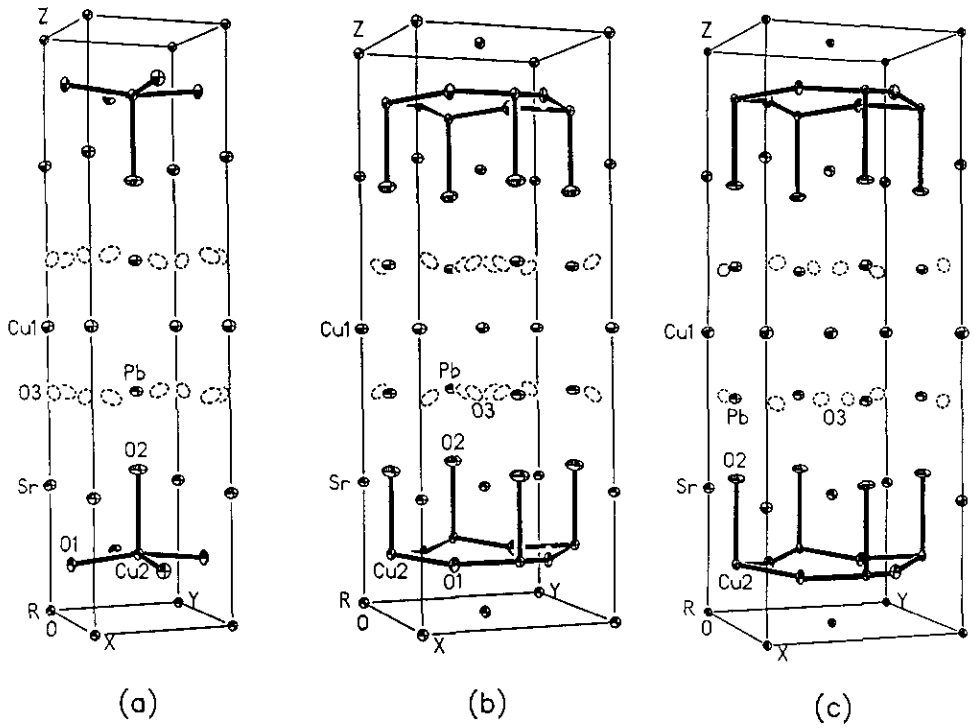

FIG. 1. Unit cells of $Pb_2Sr_2RCu_3O_8$ with (a) primitive, tetragonal symmetry for R = Eu and Dy, (b) C-centered, orthorhombic symmetry for R = La, and (c) C-centered monoclinic symmetry for R = Pr, Nd, and Tb. The thermal ellipsoids are drawn as 50% probability surfaces and the displaced O3 are represented by dashed ellipsoids.

None of the measured intensities of those reflections corresponding to the 5.4-Å cell was greater than $3\sigma(I)$. Therefore, a primitive 3.8-Å cell was assumed. The space group *P4/mmm* was deduced by using an algorithm suggested by Y. LePage (*12*)—a strategy based on identifying the three shortest twofold axes which limit the lattice symmetry and conventional cell edges. In the primary stage of refinement, the oxygens in the PbO layer were restricted to the position 2*g* (*0, 0, z*). The thermal parameters at this site were highly anisotropic: the components of U_{11} and U_{22} being about one order of magnitude higher than U_{33}, indicating that O3 are disordered in the basal plane. Two potential positions for O3 in space group *P4/mmm* are 8*r* (*x, x, z*) and 8*s* (*x, 0, z*). Both of them will allow the disordering of O3 over four sites. The refinement of O3 at 8*r* reduced the amplitudes of U_{11} and U_{22} to one-third of former values, but anisotropy was still large. Splitting the oxygen atoms has the effect of moving them directly toward the Pb atoms and gives rather short bond lengths of 2.310(35) and 1.866(34) Å for Pb-O3 and Cu1-O3, respectively. The refinement using 8*s* (*x, 0, z*) gives basically isotropic thermal displacement parameters and reasonable bond lengths of Pb-O3 and Cu1-O3 (see Table III). The O3 atoms at the 8*s* position (denoted by dashed ellipsoids in Fig. 1a) are located on the *ac* and bc planes. The unit cell is shown in Fig. 1a. Two short bonds (2.358 Å) and two long bonds (3.116 Å) of Pb-O3 indicate that the Pb ions are in

TABLE II

ATOMIC POSITIONS AND THERMAL DISPLACEMENT PARAMETERS FOR $Pb_2Sr_2RCu_3O_8$ (R = La, Pr, Nd, Eu, Tb, and Dy)

R:		La	Pr	Nd	Eu	Tb	Dy
Pb	x		0.4970(2)	0.4984(1)		0.4959(1)	
	z	0.3899(1)	0.3891(1)	0.3887(1)	0.3881(1)	0.3878(1)	0.3879(1)
	U_{11}	0.029(1)	0.019(1)	0.016(1)	0.013(1)	0.015(1)	0.013(1)
	U_{22}	0.019(1)	0.016(1)	0.014(1)	0.013	0.011(1)	0.013
	U_{33}	0.007(1)	0.007(1)	0.007(1)	0.008(1)	0.007(1)	0.007(1)
	U_{13}		0.000(1)	0.001(1)		−0.000(1)	
Sr	x		0.0018(3)	0.0015(2)		0.0051(1)	
	z	0.2219(2)	0.2223(1)	0.2221(1)	0.2211(1)	0.2210(1)	0.2209(1)
	U_{11}	0.014(2)	0.008(1)	0.014(1)	0.013(1)	0.011(1)	0.013(1)
	U_{22}	0.006(1)	0.011(1)	0.011(1)	0.013	0.010(1)	0.013
	U_{33}	0.007(1)	0.007(1)	0.008(1)	0.009(1)	0.008(1)	0.008(1)
	U_{13}		0.000(1)	0.002(1)		−0.001(1)	
R	U_{11}	0.028(2)	0.012(1)	0.013(1)	0.007(1)	0.006(1)	0.009(1)
	U_{22}	0.016(1)	0.008(1)	0.009(1)	0.007	0.005(1)	0.009
	U_{33}	0.012(1)	0.011(1)	0.008(1)	0.007(1)	0.006(1)	0.004(1)
	U_{13}		−0.002(1)	0.001(1)		−0.001(1)	
	K	1.00	1.00	1.00	0.906(7)	0.955(3)	0.911(8)
Cu1	U_{11}	0.028(4)	0.021(3)	0.012(1)	0.013(1)	0.016(1)	0.012(1)
	U_{22}	0.019(3)	0.018(2)	0.014(1)	0.013	0.013(1)	0.012
	U_{33}	0.013(3)	0.009(2)	0.012(1)	0.011(2)	0.010(1)	0.010(1)
	U_{13}		0.000(2)	0.003(1)		0.002(1)	
Cu2	x		0.5008(4)	0.5012(3)		0.5020(1)	
	z	0.1133(2)	0.1111(2)	0.1104(1)	0.1088(2)	0.1068(1)	0.1071(1)
	U_{11}	0.019(3)	0.005(1)	0.011(1)	0.007(1)	0.005(1)	0.008(1)
	U_{22}	0.006(1)	0.005(1)	0.007(1)	0.007	0.005(1)	0.008
	U_{33}	0.009(2)	0.011(1)	0.008(1)	0.010(1)	0.008(1)	0.008(1)
	U_{13}		−0.002(1)	0.001(1)		−0.001(1)	
O1	x		0.2495(14)	0.2486(10)		−0.2482(6)	
	y		0.2471(17)	0.2500(13)		0.2503(7)	
	z	0.1042(9)	0.0993(6)	0.0989(4)	0.0967(6)	0.0942(3)	0.0946(6)
	U_{11}	0.030(10)	0.008(5)	0.013(3)	0.006(3)	0.009(1)	0.014(4)
	U_{22}	0.011(5)	0.005(3)	0.009(2)	0.015(4)	0.007(1)	0.004(3)
	U_{33}	0.016(6)	0.021(5)	0.014(2)	0.016(4)	0.015(2)	0.015(3)
	U_{12}	0.001(7)	0.001(3)	0.001(2)		−0.001(1)	
	U_{13}		−0.005(4)	0.003(2)		0.001(1)	
	U_{23}		−0.004(4)	0.001(2)		−0.003(1)	
O2	x		0.5032(27)	0.4974(20)		0.5053(13)	
	z	0.2530(15)	0.2540(11)	0.2537(7)	0.2539(11)	0.2526(5)	0.254(1)
	U_{11}	0.020(14)	0.016(9)	0.020(4)	0.027(5)	0.019(3)	0.031(6)
	U_{22}	0.017(9)	0.030(8)	0.026(6)	0.027	0.024(3)	0.031
	U_{33}	0.010(9)	0.010(9)	0.007(3)	0.007(5)	0.007(2)	0.010(5)
	U_{13}		0.003(7)	0.002(3)		−0.003(2)	
O3	x	0.9315(73)	0.0346(41)	0.0293(33)	0.8542(94)	0.0548(16)	0.866(10)
	y	0.0812(51)	0.0753(35)	0.0648(44)		0.0756(17)	
	z	0.3808(25)	0.3855(13)	0.3871(13)	0.3831(26)	0.3850(7)	0.387(2)
	U_{11}	0.018(3)	0.078(16)	0.055(12)	0.048(22)	0.027(4)	0.027(15)
	U_{22}	0.001(9)	0.016(9)	0.022(10)	0.016(12)	0.012(3)	0.005(8)
	U_{33}	0.032(22)	0.008(8)	0.056(12)	0.046(23)	0.019(4)	0.038(18)
	U_{12}	0.001(18)	−0.007(11)	−0.002(8)		0.002(4)	
	U_{13}	0.003(21)	−0.002(11)	0.031(10)	0.021(19)	0.002(4)	−0.009(14)
	U_{23}	0.022(12)	0.000(8)	0.003(10)		−0.001(3)	

Note. Space groups *Cmmm* (No. 65) for R = La: Pb(0, ¼, z), Sr(0, 0, z), R(0, 0, 0), Cu1(0, 0, ½), Cu2(0, ½, z), O1(¼, ¼, z), O2(0, ½, z), O3(x, y, z); *C2/m* (No. 12) for R = Pr, Nd, and Tb: Pb(x, 0, z), Sr(x, 0, z), R(0, 0, 0), Cu1(0, 0, ½), Cu2(x, 0, z), O1(x, y, z), O2(x, 0, z), O3(x, y, z); and *P4/mmm* (No. 123) for R = Eu and Dy: Pb(½, ½, z), Sr(0, 0, z), R(0, 0, 0), Cu1(0, 0, ½), Cu2(½, ½, z), O1(0, ½, z), O2(½, ½, z), O3(x, 0, z). The anisotropic thermal displacement parameter exponent has a unit of Å^2 and takes the form: $-2\pi^2(h^2a^{*2}U_{11} + \ldots + 2hka^*b^*U_{12})$. K stands for site-occupation. The last digit, in parentheses, is the uncertainty.

TABLE III

SELECTED BOND LENGTHS (Å) AND ANGLES (°) FOR THE $Pb_2Sr_2RCu_3O_8$ (R = La, Pr, Nd, Eu, Tb, AND Dy) CRYSTALS

R		La	Pr	Nd	Eu	Tb	Dy
				Bond lengths (Å)			
Pb–O2	×1	2.172(24)	2.135(17)	2.130(10)	2.119(17)	2.144(6)	2.116(16)
–O3	×1	2.340(29)	2.338(19)	2.386(24)	2.358(21)	2.357(8)	2.375(22)
	×1	2.402(40)	2.556(22)	2.578(18)	2.358	2.401(8)	2.375
	×1	3.140(27)	2.963(20)	2.911(25)	3.116(21)	3.064(8)	3.092(19)
	×1	3.225(35)	3.160(15)	3.093(19)	3.116	3.131(8)	3.092
Sr–O1	×2	2.692(10)	2.753(9)	2.744(6)	2.748(7)	2.766(4)	2.763(7)
–O1	×2	2.692	2.731(9)	2.733(6)	2.748	2.770(4)	2.763
–O2	×2	2.797(4)	2.786(3)	2.779(2)	2.769(3)	2.766(1)	2.759(3)
	×1	2.774(4)	2.779(15)	2.744(11)	2.769	2.737(7)	2.759
	×1	2.774	2.768(15)	2.789(11)	2.769	2.756(7)	2.759
–O3	×1	2.589(40)	2.618(21)	2.630(21)	2.619(40)	2.647(9)	2.672(37)
R–O1	×4	2.549(9)	2.477(9)	2.475(6)	2.455(6)	2.425(4)	2.427(6)
–O1	×4	2.549	2.503(9)	2.487(6)	2.455	2.426(4)	2.427
Cu1–O3	×2	1.981(40)	1.865(21)	1.823(21)	1.929(40)	1.858(9)	1.849(37)
Cu2–O1	×2	1.944(1)	1.936(9)	1.928(7)	1.932(1)	1.926(3)	1.927(1)
–O1	×2	1.944(1)	1.949(9)	1.947(7)	1.932	1.932(3)	1.927
–O2	×1	2.218(25)	2.259(17)	2.261(10)	2.290(17)	2.280(6)	2.317(17)
				Bond angles (°)			
O3–Pb–O3		173.1(19)	169.5(11)	171.8(9)	176.1(20)	163.6(4)	179.5(18)
		172.9(20)	104.3(8)	101.9(7)	160.2(15)	107.5(3)	162.4(15)
		160.3(20)	104.3	101.9	109.3(15)	107.5	107.6(14)
		157.4(15)	85.7(6)	86.1(6)	89.9(1)	88.8(2)	90.0(1)
		109.7(14)			70.6(15)		72.4(14)
		91.3(10)					
		88.3(10)					
		69.9(14)					
O3–Cu1–O3		180.0(1)	180.0(1)	180.0(1)	180.0(1)	180.0(1)	180.0(1)
		158.2(23)	180.0	180.0	156.3(15)	180.0	157.4(16)
		153.9(17)	154.5(12)	157.6(15)	146.2(22)	155.7(5)	147.8(23)
		145.8(20)	154.5	157.6		155.7	
O1–Cu2–O2		94.3(4)	95.6(4)	95.8(3)	95.7(3)	96.0(2)	95.9(3)
			95.4(4)	94.9(3)		95.8(2)	
R–O1–R		99.0(5)	101.9(3)	102.1(2)	103.1(4)	104.6(1)	104.3(4)
Pb–O2–Sr		100.2(5)	101.5(6)	100.3(4)	100.8(3)	101.7(2)	101.0(4)
		100.3(5)	100.4(3)	100.3(2)		100.1(1)	
			99.3(6)	100.5(4)		98.6(2)	

a very distorted square pyramidal coordination environment which has been observed in another lead cuprate phase (Pb/Cu) $Sr_{2-x}La_xCuO_{5-\delta}$ as well (*13*). An attempt to put extra oxygens at a potential oxygen position (0, $\frac{1}{2}$, $\frac{1}{2}$) yielded an extremely high thermal displacement parameter which confirms the absence of oxygen in the Cu1 layer.

Full occupancy of the rare-earth sites was assumed in the early stage of structure refinement for $Pb_2Sr_2EuCu_3O_8$, but a large residual electron density peak (~10 e/Å^3) at the Eu site suggested that too many electrons had been assumed in the structural model. Thus, two hypothetical disordered models—those of cation vacancies and Eu^{3+}/Sr^{2+} mixed occupation—were refined independently. For the cation-vacancy model, the anisotropic thermal displacement parameters for Eu were refined concurrently with the site occupancy, and the results show a deficiency of 9.4% at Eu sites; while for the mixed-occupation model, an Eu^{3+}/Sr^{2+} ratio of 0.77/0.23 was obtained. Both refinements yield basically the same R indices and anisotropic displacement parameters of the rare-earth sites since the same number of electrons (57 e/site) are assigned to the rare-earth sites in both models. Similar results have been obtained in the case of R = Dy. At a final stage of the refinement, the largest residual electron density peak (~5 e/Å^3) in the difference Fourier map was at position (*0.4, 0.4, 0.4*) about 0.51 Å from the Pb ions. Refinement of the occupancy and the x and y coordinates of the Pb ions showed neither deviation from full occupation nor positional shifts. These residual electron densities seem to be caused by anisotropic extinction, imperfect correction for absorption, etc.

4. Chemical Analysis

The chemical composition of the $Pb_2Sr_2RCu_3O_8$ crystals was determined by inductively coupled plasma mass spectroscopy (ICP/MS). Approximately 3 mg of crystals was dissolved in 50 ml of 6N hydrochloric acid for each test and diluted with high-purity water to a final concentration of 0.5 to 3 ppm for each metal element. The experimental errors for the metal elements are of order ±2% and the results have been given in Table IV. A possible Na incorporation in the Ca-free $Pb_2Sr_2RCu_3O_8$ crystals was checked by an energy dispersive X-ray (EDX) analyzer (LINK QX-2000). The results were negative.

TABLE IV

CHEMICAL COMPOSITIONS OF THE $Pb_2Sr_2RCu_3O_8$ (R = Pr, Eu, Tb, AND Dy) SINGLE CRYSTALS DEDUCED FROM ICP/MS

R :	Pb	Sr	R	Cu
Pr	2.14(4)	1.94(4)	1.07(2)	3.00
Eu	1.79(4)	2.03(4)	0.89(2)	3.00
Tb	2.39(5)	1.89(4)	0.91(2)	3.00
Dy	2.12(4)	2.08(3)	0.95(2)	3.00

III. Results and Discussion

The structure refinements of four of the $Pb_2Sr_2RCu_3O_8$ compounds were carried out in either *Cmmm* (R = La) or *C2/m* (R = Pr, Nd, and Tb) by neglecting very weak reflections which violate the *C*-centering condition. Thus the true lattice type is certainly primitive and the refined structures represent an approximation to the true structure. The very weak reflections arise, most likely, from oxygen atoms in the PbO layers, and a definitive structure determination will require information from neutron diffraction as well. The other two structures, R = Eu and Dy, were refined in tetragonal symmetry, *P4/mmm*. The true symmetry here is either monoclinic or orthorhombic and the pseudo-tetragonal symmetry reflects (*110*) twinning which has been detected by electron diffraction (*14*) and which is the subject of an on-going study (*15*). Thus, the structures for R = Eu and Dy represent an average of the two twin components. Further discussion of microtwinning in tbese two samples is found in a later section of this paper. Although the structure refinements are subject to the shortcomings indicated above, they are of sufficient accuracy to provide reliable infor-

mation regarding electron densities at the R site and R–O1 distances which are crucial to arguments made later. This is because the R atoms occupy the origin in all of the space groups utilized and the O1 atoms are at ($\frac{1}{4}$, $\frac{1}{4}$, z) positions; even for the three monoclinic crystals where the position is (x, y, z), and x and y values are within 2σ of $\frac{1}{4}$ in all cases. In this section we present evidence for the existence of cation vacancies at the R site for R = Eu, Tb, and Dy, discuss the monoclinic distortion found for R = Pr, Nd, and Tb in terms of ordering of oxygen atoms driven by Pb^{2+} lone-pair ordering, and interpret a bond valence sum analysis of the six crystals studied.

1. Evidence for Cation Vacancies

As mentioned previously and as shown in Table II, electron density deficiencies were found at the R site for three of the crystals, R = Eu [9.4(7)%], Tb [4.5(3)%], and Dy [8.9(8)%], but not for R = La, Pr, or Nd. Our result for R = Nd is at variance with two previous structural studies of crystals with nominal composition $Pb_2Sr_2NdCu_3O_8$ (*4*, *6*). In both cases the R-site occupation was refined as the mixture $Nd_{1-x}Sr_x$ with $x \approx 0.24$, reflecting an electron density deficiency as Sr has fewer electrons than Nd. Comparison of the reported lattice parameters of those crystals which were grown from a PbO flux shows significant differences, a = 5.435(1) Å, b = 5.463(1) Å, c = 15.817(3) Å (*4*) and a = 5.437(3) Å, b = 5.472(2) Å, c = 15.797(7) Å (*6*), especially in the c parameter, with those reported for our crystal (see Table I) which was grown from a PbO/NaCl flux. In the accompanying paper (*10*) evidence is presented that a longer c-axis implies R-site vacancies. It is quite likely that the composition of the crystals is different due to different growth techniques. No independent chemical analysis was reported for the crystals of Refs. (*4*) and (*6*).

Returning to the cases R = Eu, Tb, and Dy for which dificiencies were found, it is clear that there are basically two models which might account for this observation, namely doping of that site with an atom of lower electron density such as Sr or Na from the flux or the presence of cation vacancies. It is of course impossible to discriminate between these models by refinement of occupational factors alone. EDX analysis of the crystals shows no detectable Na content, which leaves only Sr. The concentration of Sr needed is of the order ~23%, as mentioned earlier. Such an excess should be detectable by chemical methods. Table IV shows the results for ICP/MS analysis on four crystals from the same growth batches from which the crystals for structure determination were selected. There is no evidence for excess Sr at the required levels for R = Eu, Tb, or Dy and in fact the Sr content is the same within error as that for R = Pr which shows no rare-earth deficiency and no R-site electron deficiency as well. There is even some evidence that the R-site ion concentration is systematically lower for R = Eu, Tb, and Dy in comparison to R = Pr. The actual values obtained are in reasonable agreement with the refined occupations in Table II. The scatter in the Pb content in Table IV may be due to the high volatility of Pb or the presence of residual PbO flux on the crystal surfaces or in cracks.

The systematic behavior of the R–O1 bond lengths versus the ionic radii of R can also be used to discriminate between the two models. In Fig. 2 these distances are plotted as a function of the effective R^{3+} radius for eightfold coordination (*16*). Also plotted, as open circles, are the expected R/Sr–O1 distances for R = Eu, Tb, and Dy assuming 23% Sr^{2+}. The dashed line shows the calculated R–O1 distances assuming fourfold coordination for $O1^{2-}$. The best agreement between observed and calculated R–O1 distances is found when the $O1^{2-}$ (IV) radius is used to calculate R–O1. In fact the choice of a radius is somewhat arbitrary.

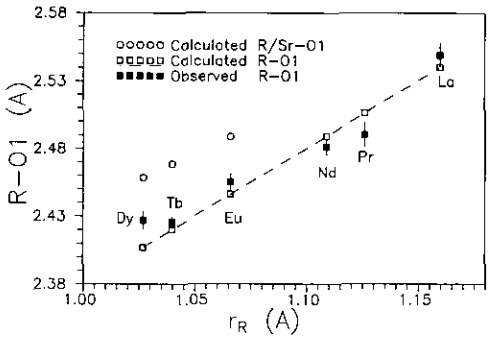

FIG. 2. Relationships between the R–O1 bond length and r_R, the effective ionic radius of R.

Although O1 has six neighbors, the distances are ~1.9 Å (2Cu), ~2.4 Å(2R), and ~2.7 Å (2Sr), thus O1 (IV) seems a reasonable compromise. It is clear that the calculated R/Sr–O1 distances are much too long, reflecting the large size of Sr^{2+}, 1.26 Å, relative to the lanthanides, 1.160 Å for La^{3+} to 1.027 Å for Dy^{3+}. This points to a further difficulty with the Sr-substitution model; i.e., it is necessary to invoke large amounts of Sr/R mixing for those cations with the largest size mismatch percentages, 16.7% for Eu^{3+} to 20.4% for Dy^{3+}. Thus, on the basis of the chemical analysis and the R–O1 bond length analysis, the R/Sr substitution model seems untenable while the cation vacancy model consistent with all experimental results.

It is worth addressing two further questions at this point. (i) Why do cation vacancies occur at the R site for these crystals, and (ii) is there any evidence for R^{3+}/R^{4+} mixed valence for R = Pr and Tb? First, the fact that vacancies appear only for the smaller rare-earths and not for the larger ones suggests a size effect. The R atoms reside in a nearly cubic site or cage formed by eight O1 atoms which are also bonded to Cu2 atoms. The cage size will be determined by factors associated with R size and Cu2–O1 bonding requirements. If the Cu2–O1 bonding is more important, then the cage size will depend more on this fact than on R size. As the rare-earth radius decreases systematically through the series, the cage volume will decrease less rapidly than the R^{3+} ionic volume and R^{3+} will fit less well into the cage. A similar situation occurs for the RMO_3 perovskites (here M stands for a transition metal) as the R radius decreases. In this case the MO_6 octahedra tilt in such a way as to decrease the size of the R–O cage with decreasing R radius. This tilting mechanism has never been observed in the layered cuprates. The creation of cation vacancies can be viewed as an alternative mechanism for decreasing the cage size and increasing the effective size of the R ion, both of which will improve the fit. A cation vacancy, having a negative formal charge, will appear "larger" in size than a cation coordinated by oxygens. Furthermore, the holes generated by the vacancy, if transferred to the Cu2–O1 network in, say, the form of formal Cu^{3+}, will shrink the Cu2–O1 bonds, decreasing the cage size. These arguments are qualitative and difficult to prove in a convincing way. Furthermore, size effects can be at most part of the explanation as the vacancies seem to result in a reproducible manner only in crystals grown from a PbO/NaCl flux. It was noted previously that the Y/Ca ratio in Ca-doped crystals grown from this flux was fixed at a roughly constant value regardless of the starting Y/Ca ratio (*2*). This might be attributed to a constant oxygen partial pressure maintained under the encapsulating NaCl layer which controls the Cu^{2+}/Cu^{3+} ratio and thus the Y/Ca ratio. A similar effect may occur in the Ca-free fluxes. Lacking a substitutional dopant ion in the absence of Ca^{2+}, the only available dopants are cation vacancies.

Regarding possible Pr^{4+}/Pr^{3+} or Tb^{4+}/Tb^{3+} admixtures at the R site, nothing truly convincing can be deduced from the results in Fig. 2. While the Pr–O1 distance seems shorter than the expected distance (dashed

line), so is the Nd–O1 distance and Nd^{4+} is an unlikely species. Also, the Tb–O1 distance is nearly identical to that of Dy–O1 suggesting that it is anomalously short, but the refined vacancy concentration in the Tb case is only half of Dy (4.5% versus 8.9%) so a valid comparison cannot be made.

2. *Monoclinic Distortion and Oxygen Ordering in the PbO Layers*

Various tetragonal, orthorhombic, and monoclinic space groups have been assigned to the Pb-2213 phase in the literature: *P4/mmm* (*17*) and *Pman* (*11*) for $Pb_2Sr_2(Y/Ca)Cu_3O_{8+\delta}$ crystals, *Cmmm* (*18*), or a combination of *Cmmm* and $P\bar{1}$ (*19*), *Pmmm* (*5*), and $P2_1/m$ (*20*) for the Ca-free 2213 compounds, and $P22_12$ (*21*) for $Pb_2Ba_2YCu_3O_8$, etc. However, the crystal structures refined in these space groups are nearly identical since all the atoms in the unit cell sit on the special positions of various space groups, except for O3 which is symmetry dependent.

Evidence for a monoclinic distortion in the $Pb_2Sr_2YCu_3O_8$ compound was first reported in the structure refinement of a powder X-ray diffraction pattern (*20*), although speculation about monoclinic symmetry had been advanced even earlier (*4*). Our structure refinements on three Ca-free $Pb_2Sr_2RCu_3O_8$ (R = Pr, Nd, and Tb) single crystals showed a definite monoclinic distortion with β values ranging from 90.13° to 90.41°. There are two major differences existing between the monoclinic (Fig. 1c) and orthorhombic structures (Fig. 1b). First of course is the monoclinic distortion in those crystals with R = Pr, Nd, and Tb

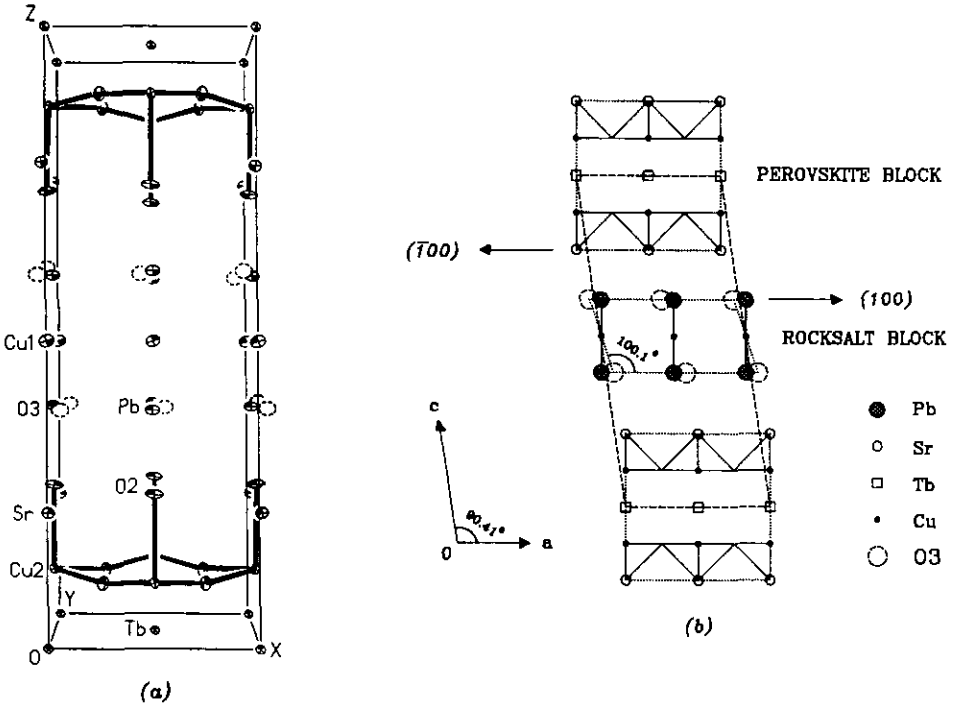

FIG. 3. (a) Three- and (b) two-dimensional (*010*) projections showing the monoclinic distortion in the $Pb_2Sr_2TbCu_3O_8$ crystal structure.

which can be seen clearly in the (*010*) projections of the unit cell as shown in Fig. 3 where both the perovskite-like (or P-) and the metal sublattice in the rocksalt-like (or RS-) units are trying to retain their orthogonality, but are shifted with respect to each other along the *a*-axis. Consequently, the bonding between the P- and RS-units are strengthened by this glide as evidenced by the short Pb–O2 and Sr–O3 bond lengths (see Table III). This contradicts, at least superficially, the observation of a preferential cleavage plane between the P- and RS-units reported by Zandbergen *et al.* (*22*). The oxygens in the lower PbO layer are shifted correspondingly along ⟨*100*⟩, and those in the upper PbO layer along ⟨$\bar{1}$*00*⟩. A serious monoclinic distortion of the oxygen (O3) sublattice in the RS-unit (with a distortion angle of 100.01° in the case of R = Tb) is thus developed. However, the driving force of this distortion roots in the Coulomb repulsion among lone pairs residing on the Pb^{2+} ions. The lone pairs of the upper PbO layer will repel those below and reorient themselves. The finding of this work is that the lone pairs point between the two Cu1 ions (see Figs. 4a and 4b) rather than toward the Cu1 ions as ascribed by Cava *et al.* (*18*). The result of this reorientation is that two in-plane O3 atoms are pushed away from the Pb^{2+} ions and form two longer Pb–O3 bonds (~3.1 Å). At the same time the other two are pushed in and the result is two short bonds (~2.4 Å). According to these hypotheses the mechanism of monoclinic distortion in the Ca-free $Pb_2Sr_2RCu_3O_8$ crystals can be summarized by the following progression:

$$\text{lone pair ordering} \rightarrow \text{distortion of O3 sublattice} \rightarrow \text{glide between P- and RS-units} \rightarrow \text{monoclinic distortion}$$

Secondly, the O3 are split into two sites in the monoclinic symmetry rather than into four sites as in the orthorhombic or tetragonal cases. Cava *et al.* (*18*) have postulated that the lone pair on Pb^{2+} is oriented roughly normal to (but directed away from) the triangular face formed by the three shortest Pb–O bonds based on the crystal structure refined in *Cmmm*. Obviously, there are a number of combinations for the direction of the lone pair in the cases of *Cmmm* and *P4/mmm* because there are four sites available for each O3 and two PbO layers in each unit

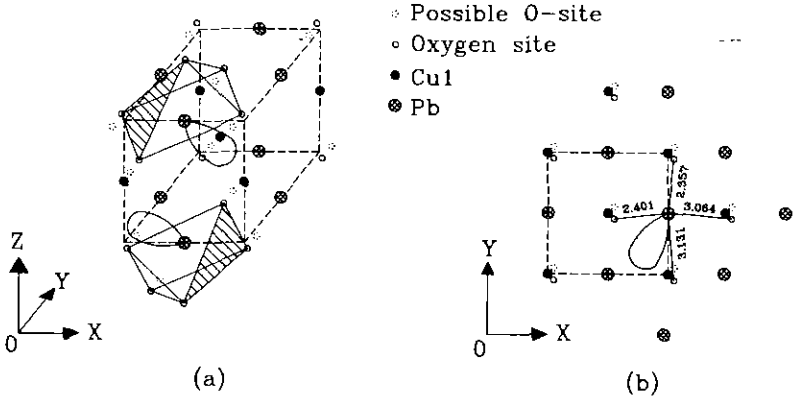

FIG. 4. (a) The lone pair of Pb^{2+} directed normal to the triangular (hatched) area composed by the three shortest Pb–O bonds, pushing two in-plane O3 away from the Pb^{2+} and resulting in a distorted square pyramid. (b) The (*001*) projection of the Cu1 and lower PbO layers showing two sets of in-plane Pb–O3 bond lengths.

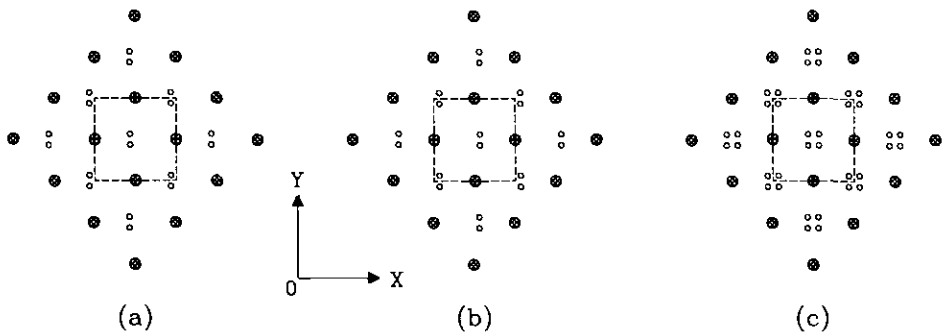

FIG. 5. Oxygen ordering of (a) the upper PbO layer, (b) the lower PbO layer in the monoclinic symmetry, and (c) the PbO layers in the orthorhombic symmetry.

cell. The situation in $C2/m$ is simpler since there are only two sites available for each O3. It is worth pointing out that the coordination environment for the Pb^{2+} ion does not change with the choice of different space groups—there are always two sets of Pb–O3 bond lengths (~2.4 Å and ~3.1 Å, cf. Table III). Thus the same postulate about the direction of the lone pair can be applied to the monoclinic case. Figures 5a and 5b show the (001) projections of the upper and lower PbO layers, respectively. By overlapping these two projections, one can obtain a familiar picture of four split O3 sites (Fig. 5c) which has been seen in the orthorhombic and tetragonal cases. This is interesting because a better oxygen ordering in the PbO layers occurs in a structure refined in the low symmetry space group $C2/m$ than that refined in the high symmetry space groups $Cmmm$ and $P4/mmm$. Further studies on the symmetry of these Ca-free crystals by the electron microscopic technique are under way.

3. *Origin of Orthorhombicity*[1] *and Possible (110) Twinning*

The origin of the orthorhombic distortion in the Pb-2213 phase has been a puzzle since the compound was discovered. Most authors believe that the displacement of O3 in the PbO layers is responsible for this distortion (*6, 18, 19*). A question raised here is: why do they displace unevenly along the a- and b-axes? The electron microscopic work conducted by Zandbergen *et al.* (*22*) shows that those reflections corresponding to the 5.4-Å cell disappear upon interaction with a strong electron beam which causes a reduction of the specimen under the high vacuum of the electron microscope, while the resultant 3.8-Å cell is still orthorhombic. This suggests that the orthorhombicity may be related to a structural distortion other than the oxygen ordering in the RS-unit, for instance, a positional shift of the Pb atoms or the tilting of CuO_6 pyramids. However, neither positional shifts nor any anomaly in the thermal parameters of Pb^{2+} or those oxygens associated with the CuO_5 pyramids have been found in our structural refinements. All known cuprate superconductors containing ions with a $5d^{10}$ configuration (without lone-pair electrons), i.e., Pb^{4+} or Tl^{3+}, are tetragonal while those containing Pb^{2+} or Bi^{3+} ($5d^{10}6s^2$), which possess lone-pair electrons, are orthorhombic. This strongly suggests that the orthorhombic symmetry in the Pb-2213 phase is correlated with the lone pair of Pb^{2+}. The source of orthorhombicity may be traced back to the synthetic process where a tetragonal

[1] The term orthorhombicity is used here to denote the situation in which $b > a$ for both orthorhombic and monoclinic symmetries.

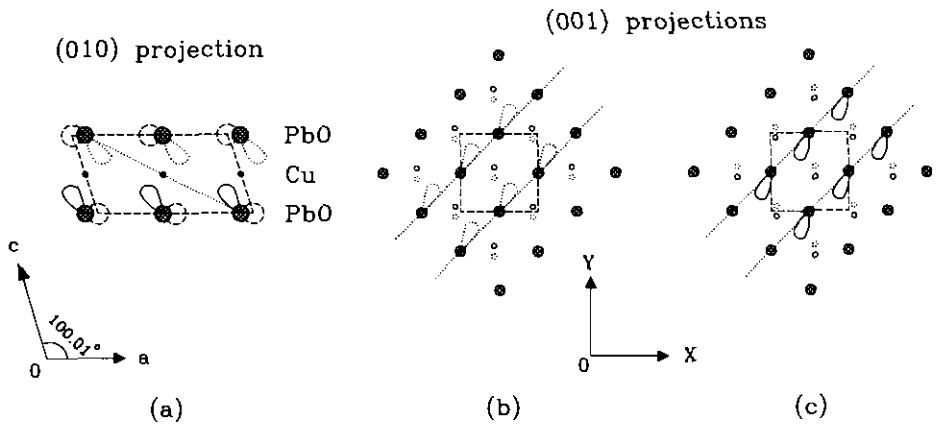

FIG. 6. The (*010*) and (*001*) projections of (a) the RS-unit, (b) the upper and (c) lower PbO layers, respectively, showing the orientation of lone pairs.

to orthorhombic phase transition for $Pb_2Sr_2GdCu_3O_8$ at 750°C upon cooling was observed by Gallagher *et al.* (*23*). Subsequently, Kadowaki *et al.* (*24*) showed a similar result for $Pb_2Sr_2(Y/Ca)Cu_3O_{8+\delta}$. Obviously, the lone pairs of the Pb^{2+} ions will be easier to fit in an expanded, high-temperature unit cell than in a smaller room-temperature cell. The thermal motion at high temperature leads to a random orientation of lone pairs. Therefore a tetragonal symmetry will be a better description for the high-temperature cell. These lone pairs start to condense into the space available in the oxygen-free Cu^1 layers upon cooling. As the temperature drops to 750°C, the distance between the two PbO layers also decreases and the strong Coulomb force triggers an ordering process among the lone pairs. Figures 6a, 6b, and 6c show the (*010*) and (*001*) projections of a possible lone-pair ordering between the upper and lower PbO layers. The uneven displacement of the O3 atoms is due to the fact that all the lone pairs in the same PbO layer align to one side of the body-diagonal line of the RS-unit as shown in Figs. 6b and 6c, and thus they will push the O3 more along the *b*- than along the *a*-axis. Since the orthorhombic structure is formed at a relatively high temperature (though lower than 750°C), it tends to maintain its integrity even when the ordering of oxygens in the PbO layers is destroyed by the strong electron beam. The O3 ordering process may initiate in different parts of a crystal, and thus a domain structure could be formed such as the (110) microtwinning observed by Hewat *et al.* (*14*). Figure 7 shows a (110) twin model which is constructed of two monoclinic domains of PbO layers. For each domain, only one out of two closely spaced oxygen sites should be filled. A possible ordering of O3 is shown in Fig. 7, where the lone pairs within one domain are oriented in the same direction and thus lower the potential energy of the crystal system. If the domain sizes are of the same order of magnitude or less than the X-ray diffraction correlation length and the volume fraction of each twin domain is nearly 50%, a tetragonal symmetry could be obtained as an average of two monoclinic domains. In this case, the tetragonal *a*-axis should be related to the monoclinic cell by $a_t = (a_m + b_m)/2\sqrt{2}$. For example, the lattice parameters of crushed crystal fragments from the same growth

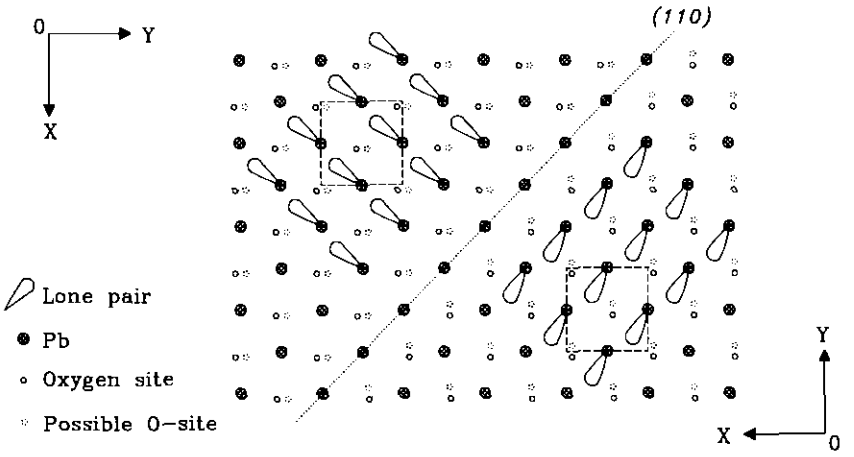

FIG. 7. Possible (*110*) twinning due to two monoclinic PbO domains.

batch as those used in the structure refinement obtained by the high-resolution Guinier powder X-ray diffraction technique are a = 5.421(1) Å and b = 5.459(1) Å for R = Eu, and a = 5.398(1) Å and b = 5.432(2) Å for R = Dy. These values are in fairly good agreement with the tetragonal lattice parameters deduced by single crystal X-ray diffraction. These observations also suggest that the twin domain size distribution is inhomogeneous within the crystals in a given batch. An attempt to deconvolve the twinning by refining a twinning parameter on the single crystal X-ray diffraction data was unsuccessful in one case (*7*). But a twin parameter of ~54% was refined on a $Pb_2Sr_2(Y/Ca)Cu_3O_8$ crystal by the single crystal neutron diffraction technique (*11*).

4. Bond Valence Sum Calculation

Bond valence sums (BVS) for each ion in the unit cell of $Pb_2Sr_2RCu_3O_8$ (R = La, Pr, Nd, Eu, Tb, and Dy) have been calculated using the expression

$$V = \sum s_i = \sum \exp[(r_0 - r_i)/\beta], \quad (1)$$

where V is the bond valence sum and is expected to equal, approximatcly, the oxidation state of the ion around which the valences have been summed. r_i and s_i are the observed bond lengths and valence of bond i, respectively, which are formed between the cations and anions. The values of r_0 and β have been calculated by Brown and Altermatt (*25*). The results for the six crystal structures refined here together with a superconducting R = Y/Ca crystal from Ref. (*17*) are shown in Table V. First, almost all of the BVS for Cu2 are higher than the formal oxidation state, +2, while the BVS for Sr and O2 are lower. Since the bond valence sum reflects the distribution of valence in thc bonds about a givcn ion, it will be increased by shortening and decreased by lengthening the bonds. Thus, the Cu2–O1 bonds in the CuO_2 planes are compressed and the Sr–O2 bonds are stretched. Furthermore, a bond valence sum of +2.0 for Pb indicates that the PbO layers are not stressed by the cell dimension constraints. Presumably, any strains in the PbO planes are relaxed by the disordering of the O3 atoms. A tension along the c-axis in the RS-

TABLE V

CALCULATED BOND VALENCE SUMS FOR $Pb_2Sr_2RCu_3O_8$ (R = La, Pr, Nd, Eu, Tb, Dy, AND Y/Ca[17]).

	La	Pr	Nd	Eu	Tb	Dy	Y/Ca
Pb	1.96	1.94	1.90	2.14	2.05	2.11	1.87
Sr	1.79	1.67	1.69	1.67	1.65	1.63	1.77
R	2.89	3.00	2.90	2.59	2.64	2.30	2.55
Cu1	0.71	0.98	1.09	0.82	1.00	1.02	0.91
Cu2	2.19	2.17	2.20	2.21	2.23	2.23	2.34
O1	−2.12	−2.13	−2.09	−2.02	−2.02	−1.95	−2.07
O2	−1.74	−1.82	−1.84	−1.83	−1.83	−1.88	−1.80
O3	−1.75	−1.75	−1.75	−1.83	−1.87	−1.86	−1.79
R/Sr				2.93	2.93	2.70	
O1				−2.11	−2.10	−2.05	

Note: Data in the last two lines are calculated in terms of the R/Sr mixed-occupation model.

units is also evidenced by the low BVS of O3. A bond valence sum close to +1.0 for the Cu1 ions is consistent with the absence of oxygen in these layers, as found in the structure refinement, since strain cannot be built up within the basal plane without Cu1–O bonds. Second, the BVS of the Cu2 ions is essentially constant as a function of R. This may seem surprising since from Table III the Cu2–O1 bond lengths clearly decrease with R. Note, however, that the Cu2–O2 bond lengths change in the opposite sense, increasing as the R radius decreases. The result is an average Cu2–O bond length of 2.00(1) Å nearly constant with R and thus a constant BVS for all six $Pb_2Sr_2RCu_3O_8$ (R = La, Pr, Nd, Eu, Tb, and Dy) crystals. Third, from the structure refinement, electron density deficiencies were found at the Eu, Tb, and Dy sites while full occupancy was obtained for R = La, Pr, and Nd. The calculated bond valence sums for La, Pr, and Nd are close to their valence state of +3 and those for Eu, Tb, and Dy are significantly less, which agree with the refinement

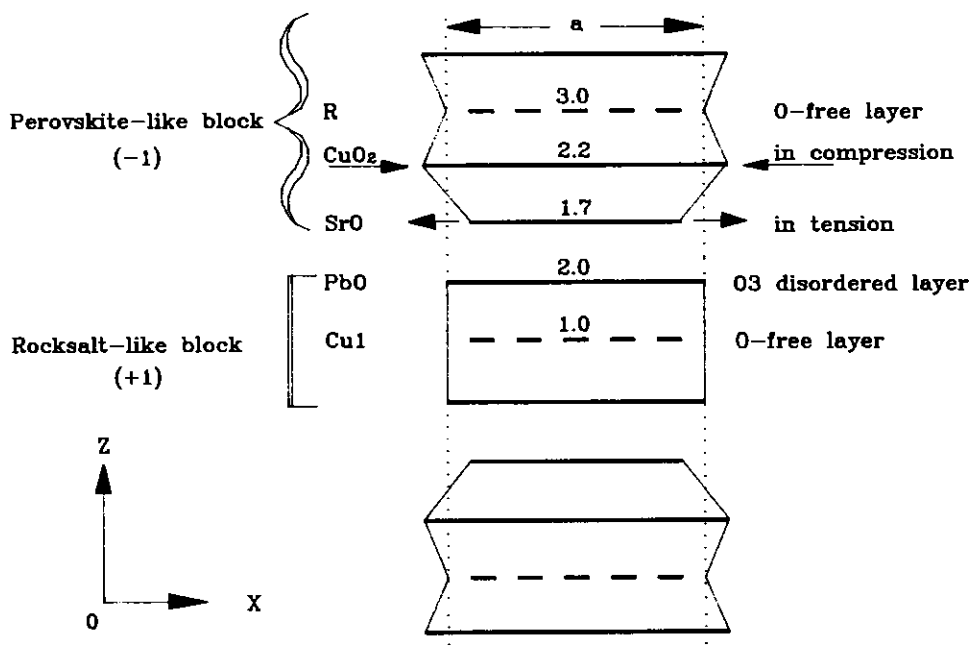

FIG. 8. Schematic diagram of generalized bond valence sums in various metal oxygen layers showing the residual strains in the crystal structure of the $Pb_2Sr_2RCu_3O_8$ compounds. The widths of the layers are exaggerated for clarity.

results and are comparable to those of R = Y/Ca crystal.

Residual strains in the crystal structure of $Pb_2Sr_2RCu_3O_8$ are illustrated schematically in Fig. 8 with the aid of generalized bond valence sums. Obviously, most strains dwell in the P-units. The R layers are strain-free due to lack of oxygen, while the compression in the CuO_2 planes is balanced by the tension in the SrO layers. Compared with the rigid P-unit, the RS-unit fits much better with the lattice dimensional constraint denoted by the two vertical dotted lines in Fig. 8 due to the flexibility supplied by the displacement of O3 and the oxygen-depleted Cu1 layers.

IV. Conclusions

Structure determinations by the single crystal X-ray diffraction technique have been performed for six crystals grown from a PbO/NaCl flux in the series $Pb_2Sr_2RCu_3O_8$, where R = La, Pr, Nd, Eu, Tb, and Dy. The presence of a significant cation vacancy concentration on the R site for R = Eu, Tb, and Dy was demonstrated. Monoclinic symmetry was established definitively for R = Pr, Nd, and Tb for the first time. The origin of the monoclinic distortion is described in terms of order/disorder among oxygens in the PbO layers which is driven by an orientational ordering of the Pb^{2+} lone pairs. The origin of microtwinning which gives rise to a pseudo-tetragonal symmetry for R = Eu and Dy is discussed. Bond valence sums show an unstressed PbO layer while the CuO_2 layers are in compression and the Sr–O layers are in tension.

Acknowledgments

One of the authors (JSX) would like to acknowledge I.D. Brown for extensive discussion regarding the bond valence sum, J. Britten for valuable assistance in the crystallographic work, N. Imanaka, and Nichia Chemical Industries Ltd. for the tCP/MS analysis. This work was supported by the Ontario Centre for Materials Research (OCMR) and by the Natural Sciences and Engineering Research Council of Canada (NSERC).

References

1. J. S. Xue, M. Reedyk, Y. P. Lin, C. V. Stager, and J. E. Greedan, *Physica C* **166,** 29 (1990).
2. J. S. Xue, M. Reedyk, A. Dabkowski, H. Dabkowska, J. E. Greedan, and C. H. Chen, *J. Crystal Growth* **113,** 371–378 (1991).
3. M. Reedyk, J. S. Xue, J. E. Greedan, and T. Timusk, *in* "Proc., 5th Annual Conference of Superconducting Applications, Buffalo, Sept. 1991"; M. Reedyk, C. V. Stager, T. Timusk, J. S. Xue, and J. E. Greedan, *Phys. Rev. B* **44,** 4539–4547 (1991).
4. R. J. Cava, B. Batlogg, J. J. Krajewski, L. W. Rupp, L. F. Schneemeyer, T. Siegrist, R. B. vanDover, P. Marsh, W. F. Peck, Jr., P. K. Gallagher, S. H. Glarum, J. H. Marshall, R. C. Farrow, J. V. Waszczak, R. Hull, and P. Trevor, *Nature* **336,** 211 (1988).
5. M. Marezio, A. Santoro, J. J. Capponi, E. A. Hewat, R. J. Cava, and F. Beech, *Physica C* **169,** 401 (1990).
6. E. A. Hayri and A. Kvick, *J. Solid State Chem.* **84,** 144 (1990).
7. L. F. Schneemeyer, R. J. Cava, A. C. W. P. James, P. Marsh, T. Siegrist, J. V. Waszczak, J. J. Krajewski, W. P. Peck, Jr., R. L. Opila, S. H. Glarum, J. H. Marshall, R. Hull, and J. M. Bonar, *Chem. Mater.* **1,** 548 (1989).
8. R. Prasad, N. C. Soni, K. Adhikary, S. K. Malik, and C. V. Tomy, *Solid State Commun.* **76**(5), 667 (1990).
9. M. Reedyk, T. Timusk, J. S. Xue, and J. E. Greedan, *Phys. Rev. B.* **45,** 7406 (1992).
10. J. S. Xue, M. Reedyk, J. E. Greedan, and T. Timusk, *J. Solid State Chem.*, **102,** 492 (1993).
11. C. Chaillout, O. Chmaissen, J. J. Capponi, T. Fournier, G. McIntyre, and M. Marezio. *Physica C* **175,** 293 (1991).
12. Y. LePage, *J. Appl. Crystallogr.* **15,** 255 (1982).
13. G. H. Kwei, P. C. Canfield, Z. Fisk, J. D. Thompson, and R. B. Von Dreele, *Physica C* **176,** 57–63 (1991).
14. E. A. Hewat, J. J. Capponi, R. J. Cava, C. Chaillout, M. Marezio, and J. L. Tholence, *Physica C* **157,** 509–514 (1989).
15. M. Hervieu, private communication.
16. R. D. Shannon, *Acta Crystallogr. A* **32,** 751 (1976).
17. M. A. Subramanian, J. Gopalakrishnan, C. C. Torardi, P. L. Gai, E. D. Boyes, T. R. Askew, R. B. Flippen, W. E. Farneth, and A. W. Sleight, *Physica C* **157,** 124 (1989).

18. R. J. Cava, M. Marezio, J. J. Krajewski, W. F. Peck, Jr., A. Santoro, and F. Beech, *Physica C* **157,** 272–278 (1989).
19. J. E. Jorgensen and N. H. Andersen, *Acta Chem. Scand.* **45,** 19 (1991).
20. H. Fujishita, S. Yamagata, and M. Sato, *J. Phys. Soc. Jpn.* **60,** 913 (1991).
21. W. T. Fu, H. W. Zandbergen, W. G. Haije, and L. J. De Jongh, *Physica C* **159,** 210–214 (1989).
22. H. W. Zandbergen, K. Kadowaki, M. J. V. Menken, A. A. Menovsky, G. van Tendeloo, and S. Amelinckx, *Physica C* **158,** 155 (1989).
23. P. K. Galagher, H. M. O'Bryan, R. J. Cava, A. C. W. P. James, D. W. Murphy, W. W. Rhodes, J. J. Krajewski, W. F. Peck, Jr., and J. V. Waszczak, *Chem. Mater.* **1,** 277–285 (1989).
24. K. Kadowaki, M. J. V. Menken, and A. C. Moleman, *Physica C* **159,** 165–172 (1989).
25. I. D. Brown and D. Altermatt, *Acta Crystallogr. B* **41,** 244 (1985).